Detection of solvated electrons below interface between atmospheric-pressure plasma and water by laser-induced desolvation

Yoshinobu Inagaki and Koichi Sasaki

Division of Applied Quantum Science and Engineering, Hokkaido University, Sapporo 060-8628, Japan

E-mail: inagaki@eis.hokudai.ac.jp

E-mail: sasaki@qe.eng.hokudai.ac.jp

Abstract. We have developed a new method to detect solvated (hydrated) electrons at the plasma-water interface. The method is based on the laser-induced desolvation followed by the release of free electrons into the plasma. We employed an atmospheric-pressure dc glow discharge, in which the water surface worked as the cathode, in the experiment. When the region just below the water cathode was irradiated with a pulsed laser beam, we observed the pulsed increase in the discharge current. The increase in the discharge current was caused by the release of free electrons which were produced from hydrated electrons by the laser-induced desolvation. The pulsed increase in the discharge current was sensitive to the laser wavelength. We compared the relationship between the pulsed increase and the laser wavelength with the distribution of the solvation energy of hydrated electrons with the help of a Monte Carlo simulation on the transport of free electrons in water. As a result, it was concluded that hydrated electrons produced at the experimental condition were located at a distance of 7-15 nm from the plasma-water interface.

The plasma-liquid (plasma-water) interaction becomes an important topic in the field of plasma chemistry as a basic research subject related with new plasma applications, such as water treatment [1–3], medicine [4–6], agriculture [7–9], and analysis [10–12]. In particular, in last several years, elaborate efforts have been put into the diagnostics of the limited region near the plasma-liquid interface. It is believed that there is a thin region with high concentrations of reactive chemical species just below the interface. The solvated (hydrated) electron, which is an electron surrounded by oriented water molecules, is one of such reactive species. Today, many scientists try to obtain the information about the energetics, the binding motifs, and the dynamics of solvated electrons by quantum mechanical calculations [13, 14] and photoelectron spectroscopy of liquid microjets [15, 16].

The reaction rate coefficients of hydrated electron have been investigated intensively in the bulk region of water mainly by pulse radiolysis and laser photolysis [17]. In contrast, the progress of the research on the nature of hydrated electron at the plasma-liquid interface is significantly insufficient to date because of the lack of useful detection methods. In 2015, Rumbach and coworkers succeeded in detecting hydrated electrons just below the interface

between water and an atmospheric-pressure plasma [18, 19]. Their detection method was laser absorption spectroscopy with the total reflection geometry, but it may be a delicate experiment since the water surface interacting with an atmospheric-pressure plasma usually vibrates. More recently, Sakakibara and coworkers detected hydrated electrons produced by laser-induced plasma in water [20], but it was not an experiment at the plasma-water interface. In previous works [21, 22], we investigated the reactivity of solvated electrons in liquids interacting with plasmas by measuring the lifetime of solvated electrons produced by the charge transfer to solvent (CTTS) transition of iodide negative ions (I^-) [23]. However, these experiments were carried out in bulk liquids, and solvated electrons we observed were not generated by the plasma-liquid interaction. Thus, another method is needed to detect hydrated electrons at the plasma-liquid interface.

In this work, we employed the laser-induced desolvation of hydrated electrons. It is known that hydrated electrons are converted into free electrons when they are irradiated with photons with energies exceeding the solvation energy, and a part of free electrons are released from the water surface [15]. Figure 1 shows the energy diagram of the laser-induced desolvation followed by the release of free electrons. In this figure, it is assumed that hydrated electrons are located at the surface of water. The solvation energy of hydrated electrons has already been investigated by Suzuki and coworkers [16, 24]. It has a Gaussian distribution given by

$$f(E) = \frac{1}{\sqrt{2\pi}\sigma} \exp\left\{-\frac{(E - E_\mathrm{c})^2}{2\sigma^2}\right\}, \tag{1}$$

where E_c and σ are the solvation energy at the peak and the standard deviation of the distribution, respectively. Suzuki and coworkers have reported $E_\mathrm{c} = -3.76$ eV and $\sigma = 0.43$ eV based on their experiment by photoelectron spectroscopy. When hydrated electrons are irradiated with laser photons with an energy E_p, they are excited toward the conduction band, as shown in Fig. 1. Hydrated electrons are desolvated and they are converted into free electrons if $E + E_\mathrm{p} \geq E_0$, where E_0 is the bottom energy of the conduction band. Although the value of E_0 is still under the discussion, we employed $E_0 = -1.2$ eV in this work [25]. Free electrons cannot escape from the liquid water if $E_0 \leq E + E_\mathrm{p} \leq 0$. On the other hand, if $E + E_\mathrm{p} \geq 0$, free electrons are released from the water surface. When the laser-induced desolvation occurs inside the liquid water at a distance from the surface, free electrons lose their kinetic energies during the highly collisional transport in the liquid water, and in this case, a smaller part of free electrons produced by the desolvation can be released from the water surface. In this work, as will be described later, we carried out a Monte Carlo simulation to examine the transport efficiency of free electrons.

Figure 2 shows the photograph and the schematic illustration of the experimental setup. A metal nozzle electrode and an NaCl solution (0.1 g/L) were installed inside a glass vessel. The inner and outer diameters of the nozzle electrode were 500 and 800 μm, respectively. The distance between the tip of the nozzle electrode and the solution surface was 1 mm, and helium was flowed from the electrode toward the solution surface at a rate of 150 mL/min. In addition, we applied another helium flow of 7 L/min into the vessel to minimize the admixture of air into the discharge. A dc voltage was applied between the electrode and the solution surface to

generate an atmospheric-pressure dc glow discharge. Note that the solution surface worked as the cathode in this dc discharge system. A ballast resistor of 25 kΩ was connected between the dc power supply and the nozzle electrode, and a shunt resistor of 50 Ω was inserted between the solution and the electrical ground. The voltage between the nozzle electrode and the platinum wire was 590-780 V, when the discharge current was varied between 7.5 and 20 mA. A roughly linear relationship was observed between the discharge voltage and the discharge current. The voltage across the shunt resistor was measured using an oscilloscope to measure the temporal variation of the discharge current. In addition to these resistors, a capacitor of 1000 pF was inserted to bypass the high-frequency current.

The interface between the plasma and the solution surface was irradiated with Nd:YAG and dye laser beams from the bottom at an incident angle of 60°. The plasma-water interface reflected the incident laser beam totally at this incident angle, as shown in Fig. 2. The wavelengths of the Nd:YAG laser were 266, 355, and 532 nm, and the wavelength range of the tunable dye laser was 280-370 nm. The durations of the laser pulses were 8 ns. The diameter of the YAG laser beam was 8 mm, whereas an elliptical orifice (3×2 mm) was used for shaping the dye laser beam. The irradiation of the laser beams from the water side at an angle for the total reflection is important to avoid the production of free electrons by photodetachment of negative ions in the plasma [26]. If the laser beam is injected into the interface from the gas side, electrons released from the water surface, which are caused by the laser-induced desolvation, are masked by electrons produced by photodetachment of negative ions. It is important to note that we can expect a proportional relationship between the flux of free electrons released from the water surface and the pulsed increase in the discharge current. This is because we observed a proportional relationship between the pulsed increase in the discharge current and the number of free electrons produced by laser photodetachment in our previous work [26].

We observed the temporal variation in the discharge current, as shown in Fig. 3, when the solution cathode was irradiated with the Nd:YAG laser beam. The laser energy was adjusted to 38 mJ/pulse at all the laser wavelengths of 266, 355, and 532 nm. The origin of the horizontal axis corresponds to the timing of the laser pulse injection, whereas the vertical axis is given by the ratio between the amplitude of the pulsed current and the dc current at the steady-state ($\Delta I/I_0$). The dc current was approximately 20 mA. The pulsed increases shown in Fig. 3 were observed only when both the plasma and the Nd:YAG laser beam were switched on. The high-frequency fluctuation observed at around the laser pulse was the electrical noise originated from the Q-switching of the Nd:YAG laser. In the experiment, we measured the waveforms with the laser beams being dumped in front of the vessel and subtracted them from the signals that were observed with the laser beam injection. In spite of this process, we could not remove the high-frequency noises from the signals completely. As shown in the figure, the discharge currents were increased abruptly by the irradiation of the Nd:YAG laser beams at 266 and 355 nm. After the disappearance of the laser beam, we observed the gentle decay in the discharge current. The increase ratios in the discharge current were 3.5% and 0.36% at 266 and 355 nm, respectively. In contrast, the pulsed increase in the discharge current was negligible, when the solution cathode was irradiated with the Nd:YAG laser beam at 532 nm,

as shown in Fig. 3.

The ratio between the amplitude of the pulsed current and the dc current is plotted in Fig. 4 as a function of the energy of the Nd:YAG laser beam. The laser wavelength was 266 nm, and the discharge current was constant at 20 mA. The plots in the figure are the averages of multiple measurements, and the error bars indicate the maximum and minimum values. The amplitude of the pulsed current increased linearly with the laser energy. Figure 5 shows the relationship between the amplitude of the pulsed current and the steady-state dc current. The wavelength and the energy of the Nd:YAG laser beam were 266 nm and 38 mJ/pulse, respectively. As shown in the figure, the amplitude of the pulsed current increased rather steeply with the dc current. Figure 6 shows the relationship between the amplitude of the pulsed current and the concentration of H_2O_2 admixed into the NaCl solution. The laser wavelength was 266 nm and the steady-state dc current was 20 mA. It is known that H_2O_2 works as a scavenger of hydrated electrons. The solid curve illustrated in the figure is given by

$$\frac{\Delta I}{I_0} = \frac{\alpha}{\nu + k[\mathrm{H_2O_2}]}, \tag{2}$$

where $[\mathrm{H_2O_2}]$ is the concentration of H_2O_2, ν is the loss frequency of hydrated electrons due to mechanisms other than the reaction with admixed H_2O_2, and α stands for the proportional constant including the production rate of hydrated electrons. The rate coefficient k is known as $k = 1.1 \times 10^{10}$ $\mathrm{M^{-1}s^{-1}}$ [17]. We assume $\nu = 8 \times 10^6$ $\mathrm{s^{-1}}$ in Fig. 6 according to our previous work [22], and Eq. (2) is normalized to the experimental data at $[\mathrm{H_2O_2}] = 0$ mM.

A possibility for the laser-induced production process of free electrons in the solution is photodetachment of negative ions. However, photodetachment of negative ions does not occur at the wavelengths of the Nd:YAG laser beams, since the solvation energies of negative ions are much higher than that of hydrated electron. Although the CTTS transition reduces the photon energy that is necessary for photodetachment, a photon energies of 6.3-7.5 and 6.2-6.7 eV are necessary for the CTTS transitions of Cl^- [27] and OH^- [28], respectively. Therefore, the production of free electrons from negative ions is not expected by the irradiation of the Nd:YAG laser beams. The experimental results shown in Figs. 3-6 are consistent with the assumption that the pulsed current is caused by the laser-induced desolvation of hydrated electrons followed by the release of free electrons. The photon energies corresponding to 266, 355, and 532 nm are 4.66, 3.50, and 2.33 eV, respectively, whereas the solvation energy of hydrated electrons has the distribution shown in Eq. (1). Therefore, almost all hydrated electrons are desolvated at 266 nm, while laser photons at 532 nm can desolvate no hydrated electrons. The experimental result shown in Fig. 4 suggests that the pulsed increase in the discharge current is originated from a one-photon process, which is consistent with the laser-induced desolvation. The production process of hydrated electrons in this experimental condition is considered to be the solvation of free electrons produced by ionization of H_2O molecules. The ionization reaction is due to the irradiation of energetic positive ions accelerated in the cathode sheath. Hence, the experimental result shown in Fig. 5 can be understood qualitatively by the laser-induced desolvation, since it is expected that the density of hydrated electrons is dependent on both the discharge current and the energy of positive

ions (or the discharge voltage). The decrease in the amplitude of the pulsed current with the concentration of H_2O_2, which is shown in Fig. 6, is consistent with the scavenging reaction of hydrated electrons with H_2O_2, indicating that the pulsed increase in the discharge current is caused by the laser-induced desolvation of hydrated electrons. Rumbach and coworkers observed the proportional relationship between the density of hydrated electrons and $[\mathrm{H_2O_2}]^{-1}$ at $10 \leq [\mathrm{H_2O_2}] \leq 200$ mM [18]. We did not observe the proportional relationship since ν was not negligible in comparison with $k[\mathrm{H_2O_2}]$ in our experiment.

We repeated the experiment shown in Fig. 3 by replacing the Nd:YAG laser with the tunable dye laser. The dc discharge current was 20 mA. The energy of the dye laser beam was adjusted to 10 mJ/pulse even though we employed various dyes to obtain the oscillation between 280 and 370 nm. The experimental result is shown in Fig. 7 as a function of the photon energy. The vertical axis is given by $(\Delta I/I_0)E_\mathrm{p}$, which is proportional to the total quantum yield of the laser-induced desolvation and the release of free electrons. As shown in the figure, the total quantum yield increased steeply with the photon energy.

The experimental result shown in Fig. 7 is obtained via the combination of the following two processes: the laser-induced desolvation of hydrated electrons and the transport of free electrons produced by the desolvation. The quantum yield of the laser-induced desolvation is determined by the photon energy, and hydrated electrons are desolvated if $E + E_\mathrm{p} \geq E_0$, as shown in Fig. 1. Hence, the quantum yield of the desolvation is given by

$$q(E_\mathrm{p}) = \int_{E_0}^{\infty} f(E - E_\mathrm{p})\mathrm{d}E = \frac{1}{2}\left\{1 - \mathrm{erf}\left(\frac{E_0 - (E_\mathrm{c} + E_\mathrm{p})}{\sqrt{2}\sigma}\right)\right\}. \tag{3}$$

The transport efficiency of free electrons is sensitively dependent on the birth place of free electrons (the location of the laser-induced desolvation) and the kinetic energy of free electrons just after the desolvation. The distribution of the kinetic energy of free electrons just after the desolvation is given by

$$f_\mathrm{K}(E) = f(E - (E_\mathrm{p} - E_0)). \tag{4}$$

We carried out a Monte Carlo simulation on the highly collisional transport process of free electrons with energies given by Eq. (4) using the track structure mode in the particle and heavy ion transport code system (PHITS) version 3.24 [29,30]. In the simulation, a cylinder of water with a radius and a height of 1000 nm was prepared in vacuum. An electron source was set on the cylindrical axis at various distances from the surface. The directional distribution of the initial velocities of electrons ejected from the source was assumed to be isotropic. We assumed the field-free condition in the solution. This is because the voltage between the birth place of free electrons and the water surface is expected to be much lower than the kinetic energies of free electrons and E_0 according to the numerical simulation reported by Shirafuji and coworkers [31]. We tracked the trajectories of electrons and examined the energies and the incident angles of electrons that arrived at the water surface. According to the Snell's law for electrons [32], the electron can pass through the water surface if the kinetic energy exceeds $|E_0| \tan^2\theta$ with θ being the incident angle. We counted the ratio of electrons that satisfied the above condition, and summarized the transport ratio of free electrons to vacuum as a function of the photon energy.

Figure 8 shows the ratio of free electrons that can pass through the water surface as a function of the photon energy. We denote this value by $\eta(E_{\rm p})$ in this paper. In the simulation, we assumed a point for the shape of the electron source, and we examined the transport ratio as a function of the distances from the water surface. As shown in Fig. 8, the transport ratio is sensitive to both the photon energy and the distance from the water surface. In addition, it is known from Fig. 8 that the transport ratio is dominated by electrons emitted from the top part, if the electron source has a range along the vertical direction.

The solid curves illustrated in Fig. 7 show the product between $q(E_{\rm p})$ and $\eta(E_{\rm p})$. The plots and the curves are normalized at the photon energy of 4.43 eV. As shown in the figure, in the range between 4 and 4.5 eV, the experimental relationship between the quantum yield and the photon energy is consistent with $q(E_{\rm p})\eta(E_{\rm p})$, if we assume the source of free electrons at a distance of 7-15 nm from the solution surface. In other words, it is suggested by the present experiment that solvated electrons produced by the irradiation of energetic positive ions to the solution surface are located at 7-15 nm from the plasma-liquid interface. On the other hand, the experimental quantum yield at photon energies below 4 eV does not coincide with $q(E_{\rm p})\eta(E_{\rm p})$. A possibility for the deviation is the contribution of partially solvated electrons to the laser-induced desolvation. Siefermann and coworkers have reported the existence of partially solvated electrons in the vicinity to the water surface [33]. Since the solvation energy of partially solvated electron is lower than that of the normal hydrated electron, the desolvation of partially solvated electrons can enhance the quantum yield at a low photon energy.

In conclusion, we have demonstrated the usefulness of the laser-induced desolvation for the detection of solvated (hydrated) electrons that are located just below the plasma-liquid interface. By comparing the experimental relationship between the quantum yield and the photon energy with the Monte Carlo simulation, we have suggested that hydrated electrons produced by the irradiation of energetic positive ions is mainly located at 7-15 nm from the plasma-liquid interface.

Acknowledgments

The authors would like to thank Naoki Shirai for useful discussion. They are also grateful to Satoshi Tomioka and Yuji Yamauchi for telling them the usefulness of the PHITS code for examining the transport process of free electrons in water. This work was supported by JSPS KAKENHI (21J11632, 20H00135, and 19K21861).

References

[1] Miichi T, Hayashi N, Ihara S, Satoh S and Yamabe C 2002 Generation of Radicals using Discharge inside Bubbles in Water for Water Treatment *Ozone Sci. Eng.* **24** 471

[2] Stará Z and Krčma F 2004 The study of H_2O_2 generation by DC diaphragm discharge in liquids *Czech. J. Phys.* **54** C1050

[3] Locke B R, Sato M, Sunka P, Hoffmann M R and Chang J-S 2006 Electrohydraulic Discharge and Nonthermal Plasma for Water Treatment *Ind. Eng. Chem. Res.* **45** 882

[4] Fridman G, Friedman G, Gutsol A, Shekhter A B, Vasilets V N and Fridman A 2008 Applied Plasma Medicine *Plasma Process. Polym.* **5** 503
[5] Kong M G, Kroesen G, Morfill G, Nosenko T, Shimizu T, Dijk J van and Zimmermann J L 2009 Plasma medicine: an introductory review *New J. Phys.* **11** 115012
[6] Weltmann K-D, Polak M, Masur K, Woedtke T von, Winter J and Reuter S 2012 Plasma Processes and Plasma Sources in Medicine *Contrib. Plasma Phys.* **52** 644
[7] Šerá B, Gajdová I, Šerý M and Špatenka P 2013 New Physicochemical Treatment Method of Poppy Seeds for Agriculture and Food Industries *Plasma Sci. Technol.* **15** 935
[8] Thirumdas R, Kothakota A, Annapure U, Siliveru K, Blundell R, Gatt R and Valdramidis V P 2018 Plasma activated water (PAW): Chemistry, physico-chemical properties, applications in food and agriculture *Trends Food Sci. Technol.* **77** 21
[9] Perni S, Liu D W, Shama G and Kong M G 2008 Cold Atmospheric Plasma Decontamination of the Pericarps of Fruit *J. Food Prot.* **71** 302
[10] Shirai N, Uchida S and Tochikubo F 2014 Influence of oxygen gas on characteristics of self-organized luminous pattern formation observed in an atmospheric dc glow discharge using a liquid electrode *Plasma Sources Sci. Technol.* **23** 054010
[11] Rumbach P, Lindsay A E and Go D B 2019 Turing patterns on a plasma-liquid interface *Plasma Sources Sci. Technol.* **28** 105014
[12] Kovach Y E, García M C and Foster J E 2019 Optical Emission Spectroscopy Investigation of a 1-atm DC Glow Discharge With Liquid Anode and Associated Self-Organization Patterns *IEEE Trans. Plasma Sci.* **47** 3214
[13] Herbert J M and Jacobson L D 2011 Structure of the Aqueous Electron: Assessment of One-Electron Pseudopotential Models in Comparison to Experimental Data and Time-Dependent Density Functional Theory *J. Phys. Chem. A* **115** 14470
[14] Coons M P, You Z-Q and Herbert J M 2016 The Hydrated Electron at the Surface of Neat Liquid Water Appears To Be Indistinguishable from the Bulk Species *J. Am. Chem. Soc.* **138** 10879
[15] Shreve A T, Yen T A and Neumark D M 2010 Photoelectron spectroscopy of hydrated electrons *Chemical Physics Letters* **493** 216
[16] Yamamoto Y, Karashima S, Adachi S and Suzuki T 2016 Wavelength Dependence of UV Photoemission from Solvated Electrons in Bulk Water, Methanol, and Ethanol *J. Phys. Chem. A* **120** 1153
[17] Buxton G V, Greenstock C L, Helman W P and Ross A B 1988 Critical Review of rate constants for reactions of hydrated electrons, hydrogen atoms and hydroxyl radicals ($\cdot$OH/$\cdot$O$^-$) in Aqueous Solution *J. Phys. Chem. Ref. Data* **17** 513
[18] Rumbach P, Bartels D M, Sankaran R M and Go D B 2015 The solvation of electrons by an atmospheric-pressure plasma *Nat. Comm.* **6** 7248
[19] Martin D C, Bartels D M, Rumbach P and Go D B 2020 Experimental confirmation of solvated electron concentration and penetration scaling at a plasma–liquid interface *Plasma Sources Sci. Technol.* **30** 03LT01
[20] Sakakibara N, Ito T, Terashima K, Hakuta Y and Miura E 2020 Dynamics of solvated electrons during femtosecond laser-induced plasma generation in water *Phys. Rev. E* **102** 053207
[21] Inagaki Y and Sasaki K 2020 Reactivity of solvated electrons in ionic liquid interacting with low-pressure plasmas *Jpn. J. Appl. Phys.* **59** 066001
[22] Inagaki Y and Sasaki K 2021 Reaction frequency of solvated electrons in water interacting with atmospheric-pressure helium plasma jet *Jpn. J. Appl. Phys.* **60** 096001
[23] Blandamer M J and Fox M F 1970 Theory and applications of charge-transfer-to-solvent spectra *Chem. Rev.* **70** 59
[24] Luckhaus D, Yamamoto Y, Suzuki T and Signorell R 2017 Genuine binding energy of the hydrated electron *Sci. Adv.* **3** e1603224
[25] Bernas A, Ferradini C and Jay-Gerin J-P 1997 On the electronic structure of liquid water: Facts and reflections *Chem. Phys.* **222** 151
[26] Sasaki K, Hosoda R and Shirai N 2020 Negative ion species in atmospheric-pressure helium dc glow

discharge produced in ambient air *Plasma Sources Sci. Technol.* **29** 085012
[27] Rabinowitch E 1942 Electron Transfer Spectra and Their Photochemical Effects *Rev. Mod. Phys.* **14** 112
[28] Jortner J, Raz B and Stein G 1961 Spectrum and Radius of OH^- in Solution *J. Chem. Phys.* **34** 1455
[29] Sato T, Iwamoto Y, Hashimoto S, Ogawa T, Furuta T, Abe S, Kai T, Tsai P-E, Matsuda N, Iwase H, Shigyo N, Sihver L and Niita K 2018 Features of Particle and Heavy Ion Transport code System (PHITS) version 3.02 *J. Nuclear Sci. Technol.* **55** 684
[30] Kai T, Yokoya A, Ukai M, Fujii K and Watanabe R 2015 Thermal equilibrium and prehydration processes of electrons injected into liquid water calculated by dynamic Monte Carlo method *Radiation Phys. Chem.* **115** 1
[31] Shirafuji T, Nakamura A and Tochikubo F 2014, Numerical simulation of electric double layer in contact with dielectric barrier discharge: Effects of ion transport parameters in liquid *Jpn. J. Appl. Phys.* **53** 03DG04
[32] Gaylord T K and Brennan K F 1989 Electron wave optics in semiconductors *J. App. Phys.* **65** 814–20
[33] Siefermann K R, Liu Y, Lugovoy E, Link O, Faubel M, Buck U, Winter B and Abel B 2010 Binding energies, lifetimes and implications of bulk and interface solvated electrons in water *Nat. Chem.* **2** 274

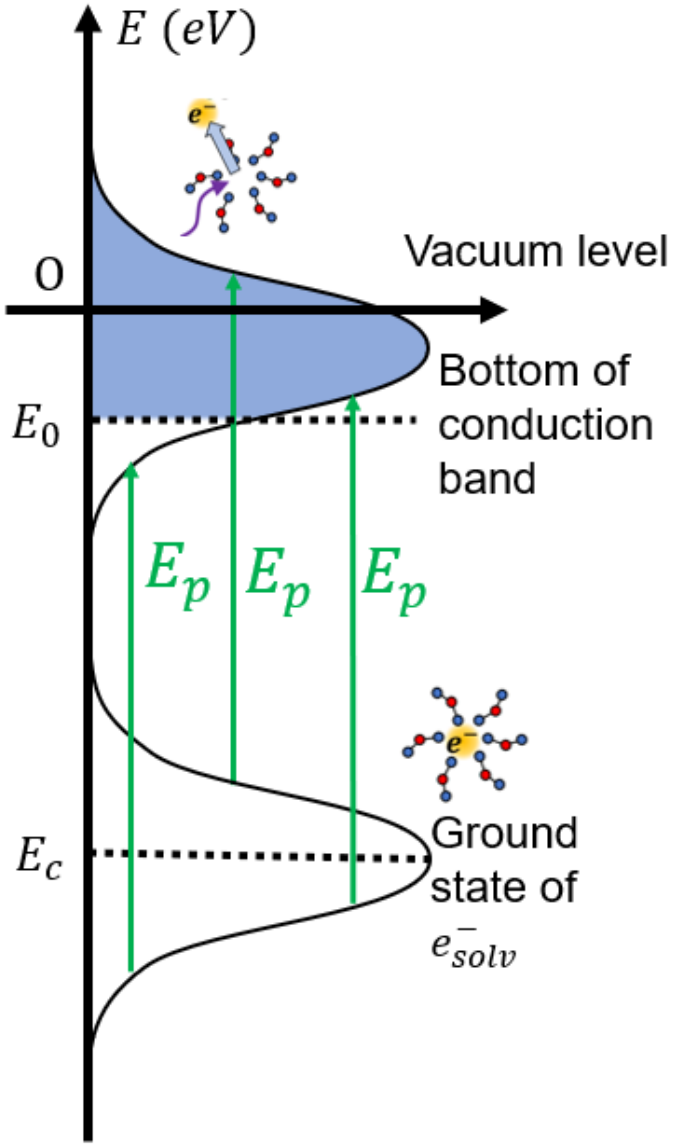

Figure 1. Energy diagram of laser-induced desolvation.

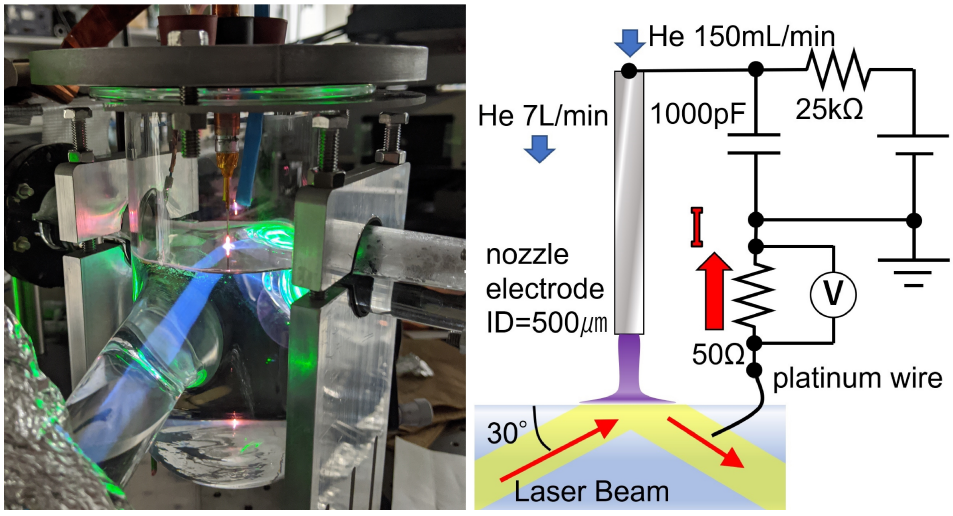

Figure 2. Photograph and schematic of the experimental setup.

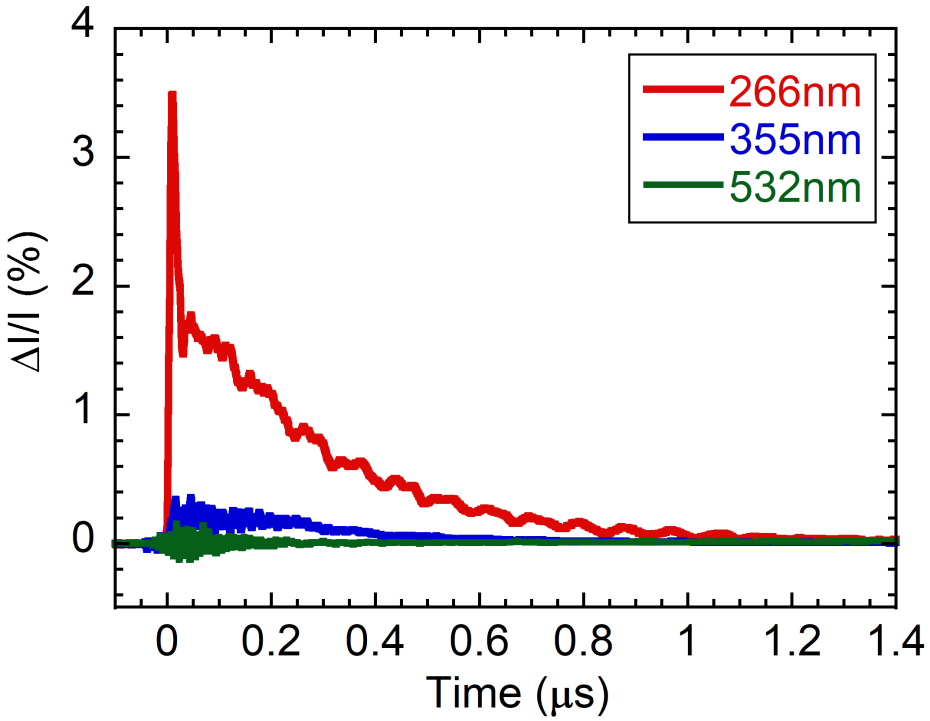

Figure 3. Temporal variations of the discharge current when the plasma-solution interface was irradiated with Nd:YAG laser beams at wavelengths of 266, 355, and 532 nm.

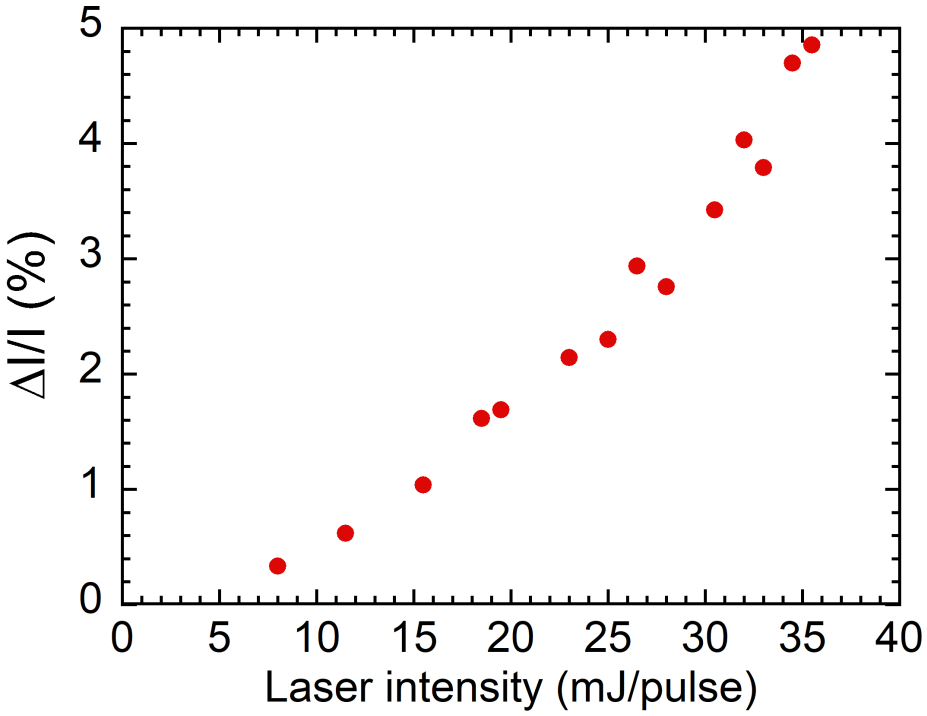

Figure 4. Ratio between the amplitude of the pulsed current and the dc current as a function of the energy of Nd:YAG laser beam at a wavelength of 266 nm

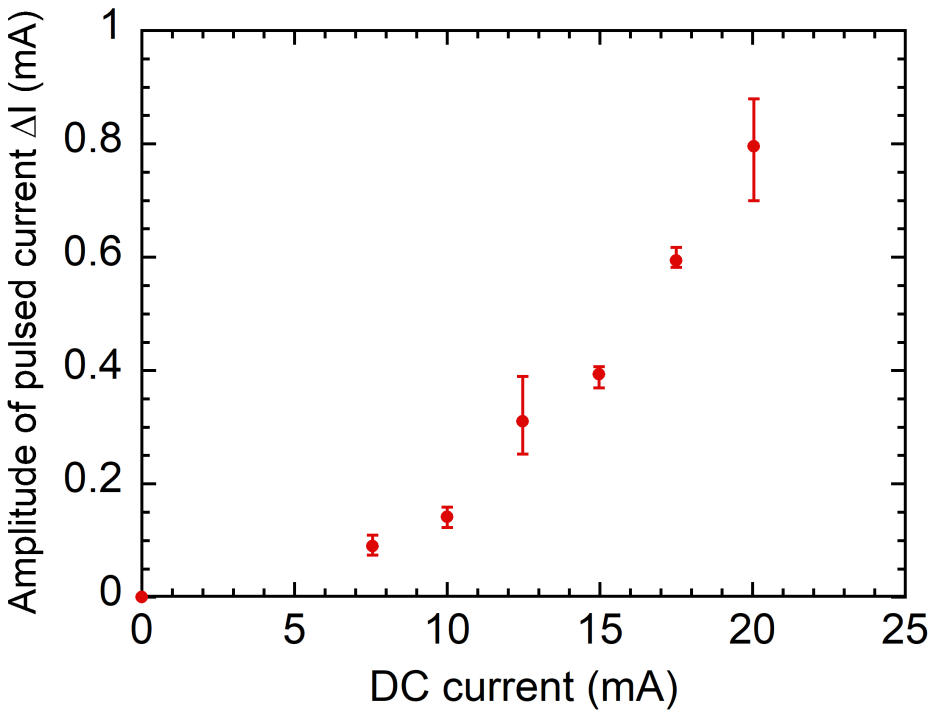

Figure 5. Amplitude of the pulsed current as a function of the dc current. The wavelength and the energy of the Nd:YAG laser beam were 266 nm and 38 mJ/pulse, respectively.

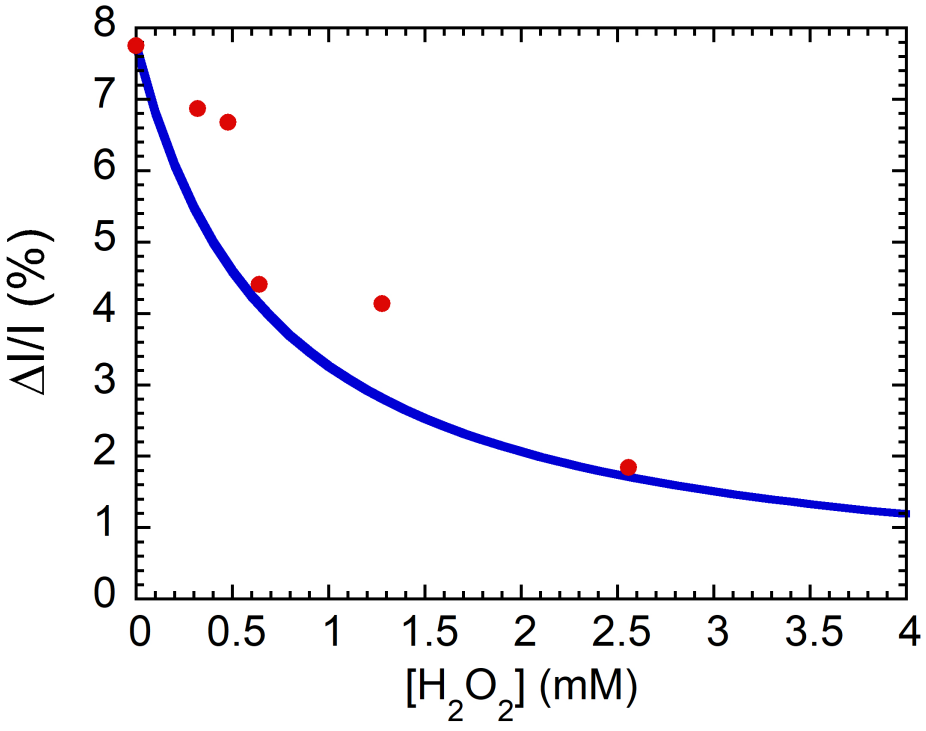

Figure 6. Amplitude of the pulsed current as a function of the concentration of H_2O_2. The wavelength and the energy of the Nd:YAG laser beam were 266 nm and 38 mJ/pulse, respectively, and the dc current was 20 mA.

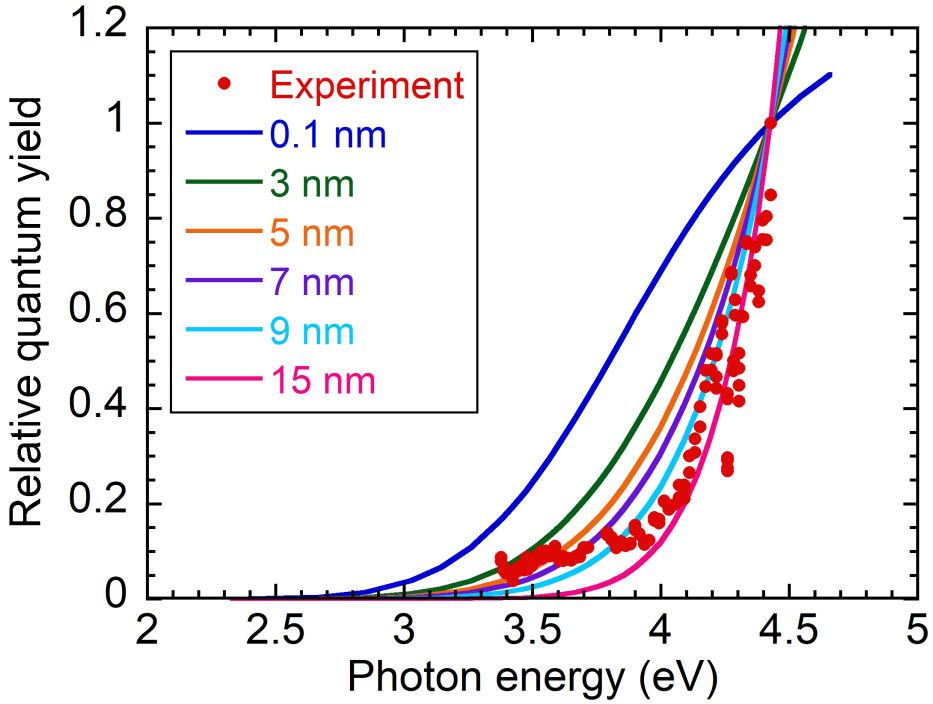

Figure 7. Comparison between the experimental result and the Monte Carlo simulation for the total quantum yield of the laser-induced desolvation followed by the release of free electrons.

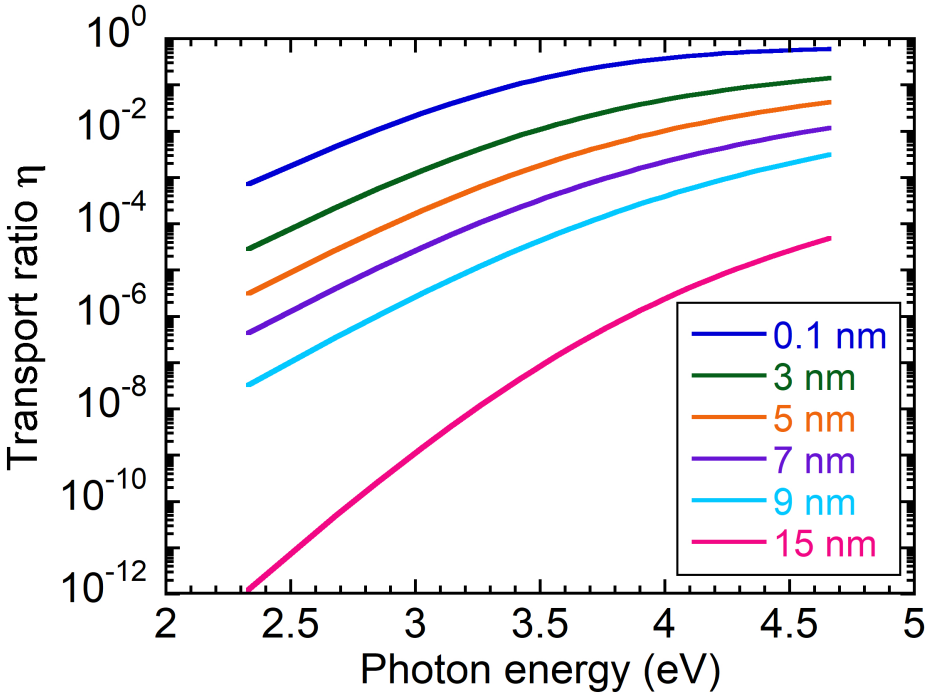

Figure 8. Result of Monte Carlo simulation showing the ratio of electrons transported to vacuum.